Beamline 10.3.2

Environmental and Materials Science, Micro X-Ray Absorption Spectroscopy

Deciphering Ni sequestration in soil ferromanganese nodules by combining X-ray fluorescence, absorption and diffraction at micrometer scales of resolution

A. Manceau[1,2], M.A. Marcus[1], N. Tamura[1], R.S. Celestre[1], A.A. MacDowell[1], R.E. Sublett[1], H.A. Padmore[1]
[1]Advanced Light Source, Lawrence Berkeley National Laboratory, Berkeley, CA 94720
[2]Environmental Geochemistry Group, Hilgard Hall, University of California, Berkeley, CA 94720

Soils are a major sink for anthropogenic Ni, and its migration to living organisms is an environmental concern because of its suspected carcinogenicity when it is speciated as nickel sulfate or combinations of nickel sulfides and oxides, provoking lung and nasal cancers. The anthropogenic nickel sources are the metal processing operations, the combustion of coal and oil, and amendments by sewage sludge. The crystal chemistry of nickel in oxidized and silicated ores has been abundantly studied for economic reasons, and in these formations Ni is predominantly associated with phyllosilicates and the Fe oxyhydroxide, goethite (α-FeOOH). During its journey from the source to its resting place in soils, Ni can undergo many chemical transformations, and understanding how this element is naturally sequestered helps provide a solid scientific basis for maintaining soil quality and formulating educated strategies to remediate severely impacted areas. The most efficient and durable process responsible for trace metal sequestration in soils is the formation of ferromanganese micronodules, which often have been compared to the well-known oceanic Mn nodules. In this work, we have studied how nickel is sequestered in soil nodules from the Morvan region (France) by combining, for the first time, scanning X-ray microfluorescence (μSXRF), microdiffraction (μSXRD), and extended X-ray absorption fine structure (μEXAFS) spectroscopy, all applied at the micrometer-scale of resolution. The two first techniques were used to identify the host solid phase by mapping the distributions of elements and solid species, respectively. μEXAFS was then used to determine the mechanism of Ni binding by the host phase at the molecular scale. We showed that nickel substitutes for Mn^{3+} in the manganese layer of the MnO_2-$Al(OH)_3$ mixed-layer oxide lithiophorite. The affinity of Ni for this mineral was subsequently found to be characteristic of micronodules sampled from soils across the USA and Europe. Since many natural and synthetic materials are heterogeneous at nanometer to micrometer scales, the unprecedented synergistic use of μSXRF, μSXRD, and μEXAFS is expected to have broad applications to earth and materials science.

RESULTS AND INTERPRETATION

With μSXRF (three first maps) the distribution of Fe, Mn, and Ni were first determined, and it was found that Mn and Ni were systematically associated in the six different soil nodules examined in this study. Then, mineral abundance maps were produced by integrating at each point-of-analysis the diffracted intensities of the non-overlapping (020) and (200) reflections at ~4.45 Å and ~2.57 Å for phyllosilicate, the (101) and (301) reflections at 4.19 Å and 2.69 Å for goethite, the (001) reflection at 7.1-7.2 Å for birnessite, and the (001) and (002) reflections at 9.39 Å and 4.69 Å for lithiophorite. The reliability of this quantitative treatment was verified by comparing mineral maps calculated using independent (*hkl*) reflections of the same mineral species. The distribution of Fe-vernadite, a common soil mineral, was not mapped because it was systematically detected throughout the examined nodules without significant gradient of concentration. This Fe-Mn disordered phase (also termed Mn-feroxyhite), that is dispersed throughout the nodule matrix filling pores and aggregating coarse grains, acts as a cementing agent for the nodules.

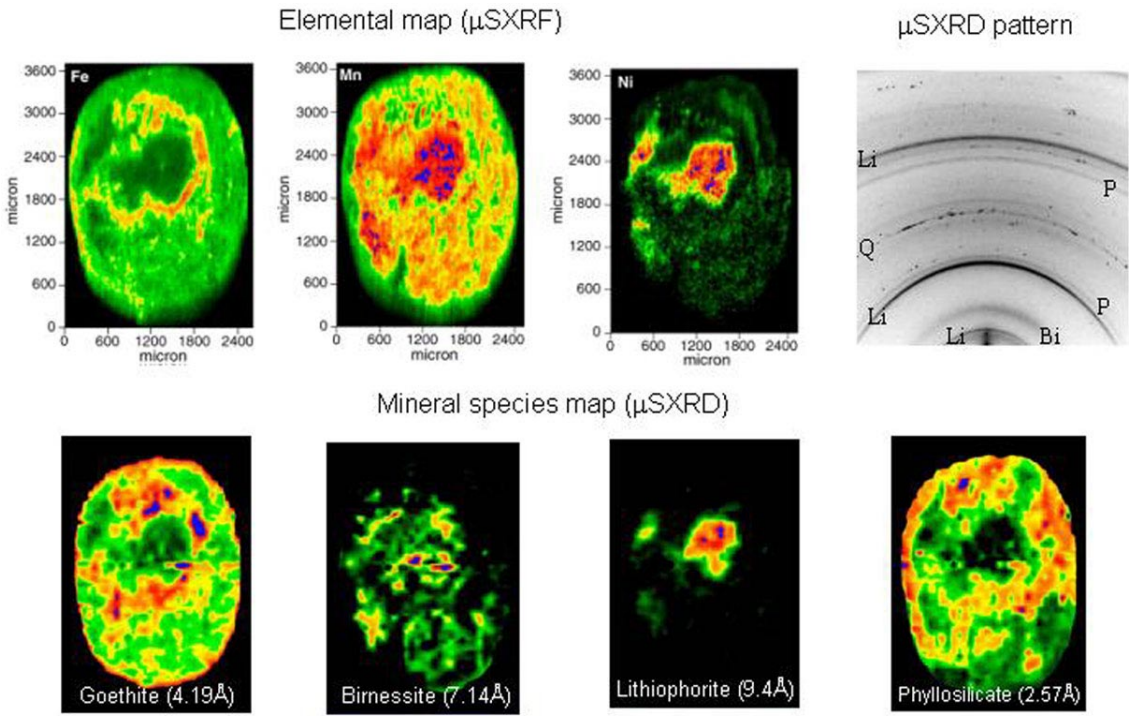

Figure 1. Combined fluorescence - diffraction measurements recorded at Beamline 7.3.3. on a ferromanganese soil nodule. The three images on the top are elemental maps obtained by µSXRF, and the four images on the bottom are mineral species maps obtained by integrating at each point of analysis the intensities of the relevant (*hkl*) reflections along the Debye rings of the two-dimensional XRD patterns (d-spacings are indicated in parenthesis). One XRD pattern is presented to the top right. Li = lithiophorite, Bi = birnessite, P = phyllosilicate, Q = quartz.

The comparison of the µSXRF and µSXRD maps clearly shows that nickel and lithiophorite have the same contour maps, therefore suggesting that Ni is bound to this particular mineral phase. The systematic association of Ni-lithiophorite suggests that Ni should be located in a definite cation site of the manganese oxide crystal structure. To determine the Ni site, Ni K-edge µEXAFS spectra were collected on Beamline 10.3.2. in Ni 'hot spots' from several nodules. All spectra were identical, indicating that the incorporation mechanism of nickel is unique, and is the key to understanding its sequestration in soils. Qualitative information about the local structure of Ni can be obtained by comparing the unknown µEXAFS spectrum to reference EXAFS spectra from relevant model compounds. As expected from µSXRF – µSXRD experiments, the two reference spectra for Ni in goethite and phyllosilicate did not match the unknown spectrum, confirming that Ni is not sequestered in these forms (data not shown). Differences in frequency and shape of the EXAFS oscillations were also observed with birnessite, in which Ni is sorbed above vacant Mn sites, and with lithiophorite, in which Ni is located within the gibbsitic Al layer (Fig. 2a). The radial structure functions (RSFs) obtained by Fourier transforming EXAFS spectra for the reference and the soil lithiophorite both exhibit, after the first oxygen peak, a second peak at roughly $R + \Delta R = 2.6$ Å, that is at a distance characteristic of edge-sharing linkage between metal octahedra (Fig. 2b). This result alone suggests that Ni is located within one of the two octahedral layers of the lithiophorite structure. To solve this alternative, suffice it to examine the phase of the imaginary part of the Fourier transform, because waves backscattered by Al and Mn atoms are almost out-of-phase. Examination of Fig. 2c shows that the unknown and lithiophorite reference have their electronic waves shifted by $\sim\pi$ in the 2.2 – 3.1 Å $R + \Delta R$ interval, thus indicating that Ni is substituted for Mn in the soil lithiophorite. In keeping with this conclusion, the two waves

are logically in phase in the 1.0 – 2.2 Å R + ΔR interval, since in both structures Ni is octahedrally coordinated to oxygen atoms.

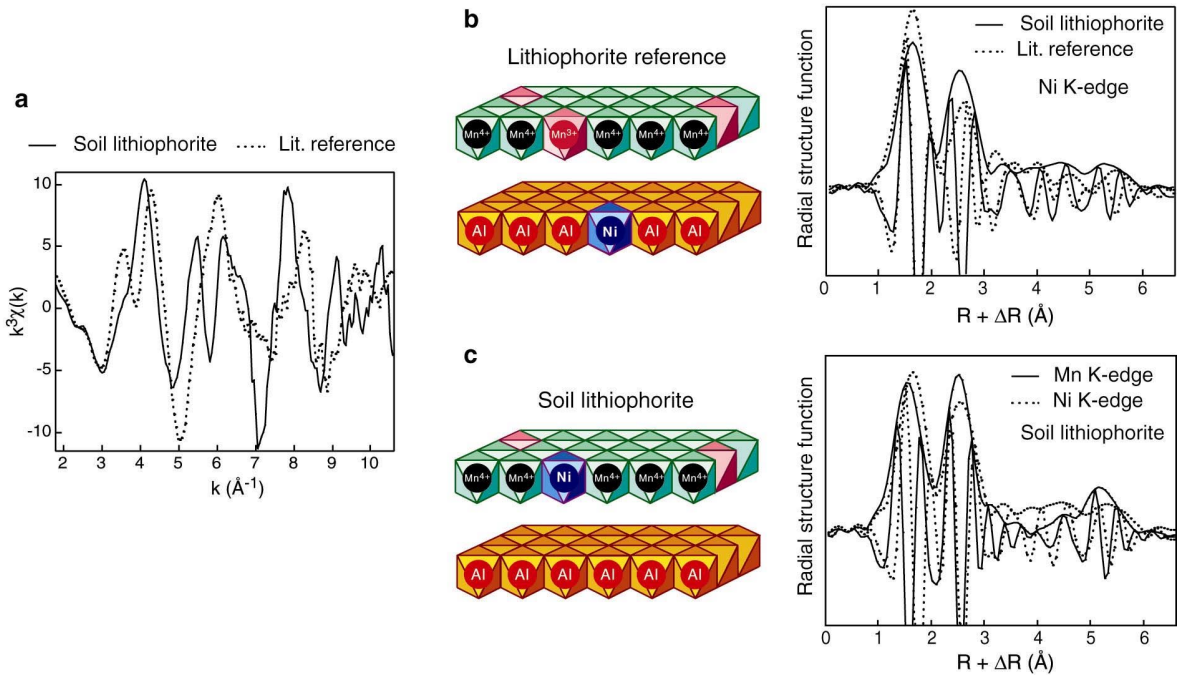

Figure 2. Ni K-edge μEXAFS spectrum (**a**) and Fourier transform (modulus plus imaginary part) (**b,c**) from a 'hot spot' of the core of the nodule, compared to the Ni- and Mn-edge data from a Ni-containing lithiophorite reference, in which Ni substitutes for Li in the $Al(OH)_3$ layer. Data were collected on Beamline 10.3.2.

Since Ni^{2+} has an effective radii 30% greater than Mn^{4+}, one may wonder how the Ni-Mn substitution is realized. To answer this question, Ni- and Mn-RSFs were plotted together (Figure 2b, bottom right), and the Ni- and Mn-EXAFS interatomic distances compared. A distinct feature in the Ni-RSF is the shift to higher R + ΔR values of the Ni-O peak, indicative of a relaxation of the Ni site owing to the larger ion size of the Ni^{2+} impurity (r = 0.69 Å) relative to Mn^{4+} (r = 0.53 Å) and Mn^{3+} (r = 0.645 Å). Since Ni^{2+} and Mn^{3+} have a size mismatch of only 7%, nickel likely substitutes on the trivalent manganese site. Likewise, the Al^{3+} site of the gibbsitic layer is clearly too small (r = 0.535 Å) to accommodate Ni^{2+}, and the larger Li^{+} site (r = 0.76 Å) is probably energetically less favorable. This assumption is supported by recent atomistic calculations and EXAFS measurements on lanthanide-doped perovskite, which showed that the rare earth is energetically stabilized in smaller crystallographic sites. A best fit to our data was given by octahedral coordination of nickel with oxygen at 2.05 Å and six manganese at 2.91 Å, and average Mn-O and Mn-Mn distances of 1.92 Å and 2.92 Å, respectively. There was no indication of Ni-Ni pairs, for which Ni-Ni distances of 3.03 Å to 3.12 Å would be predicted. This result indicates that nickel did not precipitate as a hydroxide, hence confirming that the next-nearest coordination shell of Ni is made of Mn atoms. Similar results were obtained on nodules from flood plain soils in the USA, which suggests that the Ni species identified herein may correspond to a major sequestration form of Ni in Earth near-surface environments.

This work was supported by the LBNL Laboratory Director's Research and Development Fund and by the US Department of Energy, Office of Basic Energy Sciences, under contract # DOE-AC03-765F00098.

Principal investigator: Alain Manceau, Advanced Light Source, Ernest Orlando Lawrence Berkeley National Laboratory. Email: acmanceau@lbl.gov. Telephone: 510-643-2324.

Investigation of calcifications in breast tissue using EXAFS and XRF

D.E. Sayers[1], M.Z. Kiss[1], A.C. Thompson[2], M. Marcus[3]
[1]Department of Physics, North Carolina State University, Raleigh, North Carolina 27695
[2]Advanced Light Source Division, Ernest Orlando Lawrence Berkeley National Laboratory, University of California, Berkeley, California 94270
[3]Center for X-Ray Optics, Ernest Orlando Lawrence Berkeley National Laboratory, University of California, Berkeley, California 94270

EXAFS studies have recently been conducted on calcifications in breast tissue as part of an ongoing study in the connection of calcifications to breast cancer. It has been determined that the chemical composition of calcifications is related to the development of benign or malignant breast disease [1, 2]. We are interested in improving the understanding of this connection. For our initial experiments, calcifications were removed from non-cancerous breast tissue and scanned using the EXAFS setup on beamline 10.3.2. EXAFS spectra were collected from several regions in the samples and compared to the standard spectra of hydryoxy apatite, calcium oxalate, monetite, and brushite. Figure 1 is an example of our initial results. The XANES spectra from four regions on one sample are compared with hydroxy apatite. It is clear that region A most closely resembles the hydroxy apatite spectrum. The other regions display other features in the spectra that are not present in hydroxy apatite and have not yet been accounted for in the other standards. The presence of other compounds in the calcification is a possibility, though it is not clear what role they play.

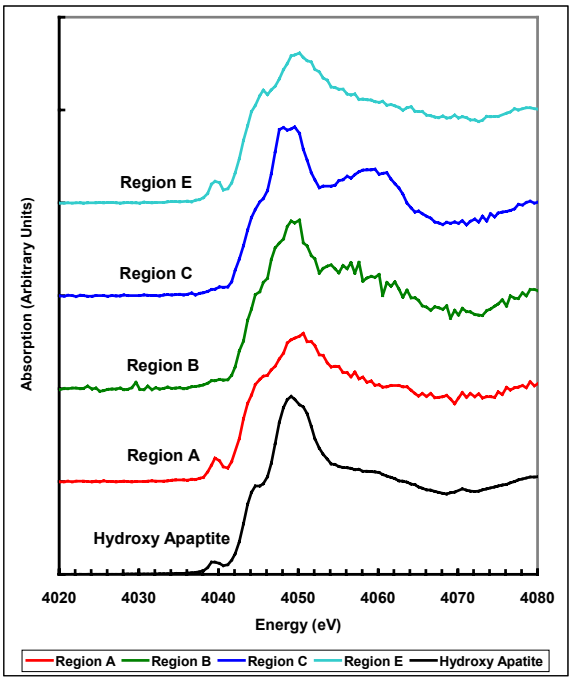

Figure 1. XANES spectra of four regions on a calcification sample from breast tissue, taken at the Ca edge. The four regions are compared to the XANES spectrum of hydroxy apatite

Additionally, XRF studies have been conducted on these tissue samples to investigate the elemental distribution in the calcifications. These studies were run concurrently on beamline 10.3.1. Figure 2 is a photo of one of the samples with the location of the calcification indicated by the dashed lines. Figure 3a is a map of the calcium concentration of this sample. The highest

concentration occurs in the region of the calcification. Other elements were present in the sample, and figure 3b shows the zinc concentration. There is a clear correlation between the calcium and the zinc with the calcium concentration roughly five times that of the zinc. None of the standards studied using EXAFS contained zinc, suggesting that this sample may contain compounds not normally associated with calcifications.

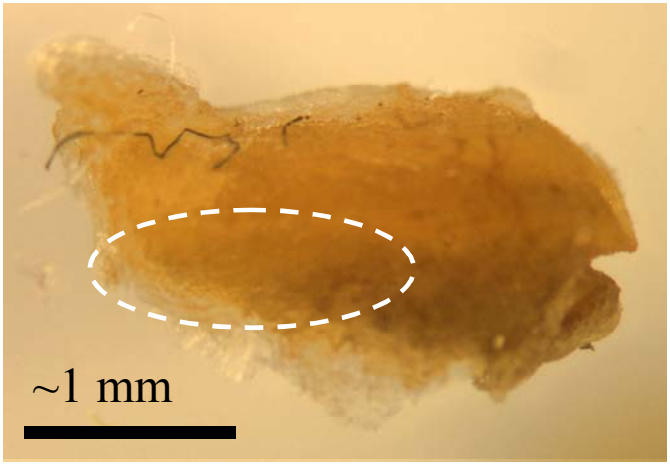

Figure 2. Photograph of one of the tissue samples. The dashed lines enclose the region of the calcification.

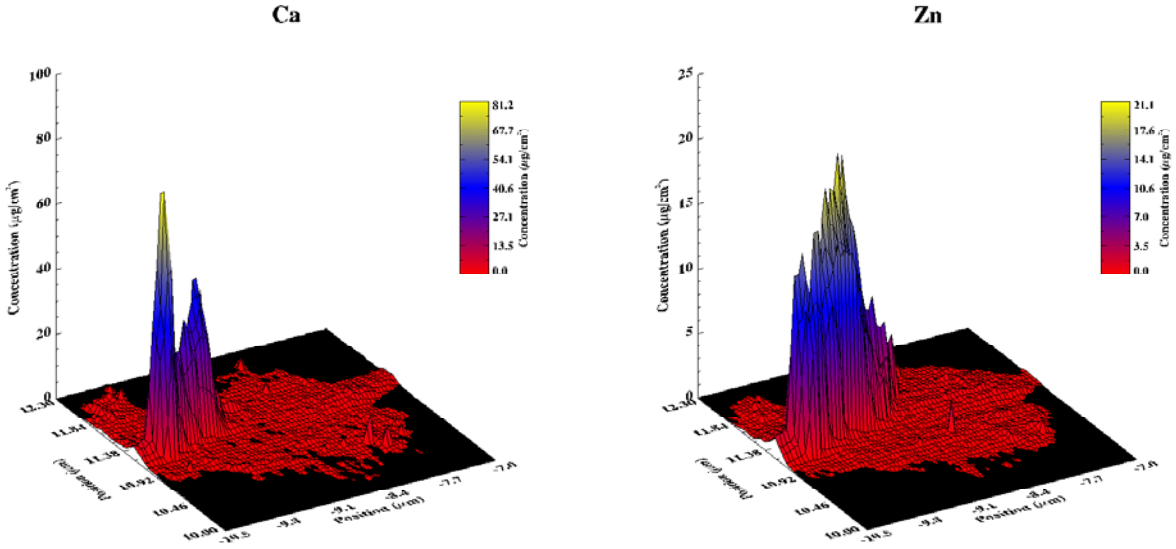

Figure 3. Concentration maps of a) Ca and b) Zn from the sample shown in figure 2.

References:

1. A. Fandos-Morera, M. Prats-Esteve, J.M. Tura-Soteras, A. Traveria-Cros, Radiology, **169**, 325 (1988).
2. M.J. Radi, Arch. Pathol. Lab. Med., **113**, 1367 (1989).

Funding Source: North Carolina State University
Contact Person: Miklos Z. Kiss, Department of Physics, North Carolina State University, email: mzkiss@unity.ncsu.edu, phone: (919) 515-5017

MicroXAFS studies into the oxidation states of different coloured glazes originating from the early Islamic world

A.D.Smith[1], T.Pradell[2], J. Molera[3], M.Vendrell[3], M.Marcus[4] and E.Pantos[1]

[1]CLRC Daresbury Laboratory, Daresbury, Warrington Cheshire, WA4 4AD United Kingdom
[2] ESAB- CEIB Universitat Politècnica de Catalunya c)Urgell 187. 08036 Barcelona Spain
[3] Departament de Cristal·lografia i Mineralogia. Universitat de Barcelona, c)Martí Franqués s/n. 08028-Barcelona
[4]Advanced Light Source, Ernest Orlando Lawrence Berkeley National Laboratory,
University of California, Berkeley, California 94720, USA

INTRODUCTION

The use of SR and SR based techniques to the study of old artifacts is a new research area [1]. Many of the techniques that are commonly used in the pursuit of contemporary material science are equally applicable to advancing an understanding of the material sciences exploited by peoples of an earlier age. Traditionally this information has been obtained from excavations and inscriptional evidence and in the case of many items such as the fine glazed ware has relied on the connoisseurship of art historians. An enhanced understanding of early materials processing techniques will enable archaeologists to better understand the societies that produced, traded and used the objects they have left behind.

We are particularly interested in investigating the lustre finish applied to ceramic ware first developed in the Islamic world of the 10^{th} to 12^{th} centuries[2-7]. Evolved techniques were subsequently developed in the Hispano Moresque world of the 13^{th} to 15^{th} centuries and later exported to Italy (in the Italian maiolica of the 16^{th} and 17^{th} centuries). The use of lustre decorated ceramics is one of the most exciting developments in pottery production during medieval times. This type of decoration consists of drawings with a metallic shine layer which was applied on a glaze, the production of which involved a second or third firing in special kilns in successive reductive steps to allow the reduction of Cu salts to the metallic state.

The lustre production reached a higher stage in the 13th and 14th century in Spain, following the Islamic tradition started in the East some centuries previously. That this was an advanced technique creating highly prized items is illustrated as the archaeological findings indicate that the majority of the Islamic and Hispano Moresque productions of these centuries were exported abroad

Different recipes allowed potters to obtain several colours and hues, such as those exhibited by the Italian maiolica (16th and 17th century.) where the lustre shows colours from copper-like to gold-like or greenish. But the typical lustre recipes from the Islamic and Hispano Moresque worlds have used copper and silver, among other non metallic components. A clue to the complexity of the manufacturing process lies in the number of “non-metallic” lustre layer specimens that have been found, implying that although the potter had intended to produce a metallic lustre, he had no success. One of the questions arising about this pottery is to determine why the colour of a particular piece did not reach the metallic shine. XRD shows that metallic Cu is present in those samples which exhibit a metallic shine, but not in the “non-metallic” examples. We consider that there are two possibilities: firstly that the reduction was not enough to obtain metallic Cu, or alternatively that the metal has formed into crystals too small to exhibit metallic

optical properties. Moreover, the distribution of copper and silver in the luster layers is not even. Silver appears in spots of some hundreds of microns where some copper is also found; copper and silver are not evenly distributed at the edges of the luster decorations. Both are also related to differences in the final colour and metallic shine.

The newly rebuilt microXAFS beamline 10.3.2 has been utilised to determine the spatial distributions of the Cu oxidation states both within areas of a constant colour and in different coloured specimens. Fluorescence microXAFS is an important technique and has enabled us to penetrate the predominately Al and Si surface layer (of the order of 100Å – 200 Å thick) to probe the metal glaze beneath.

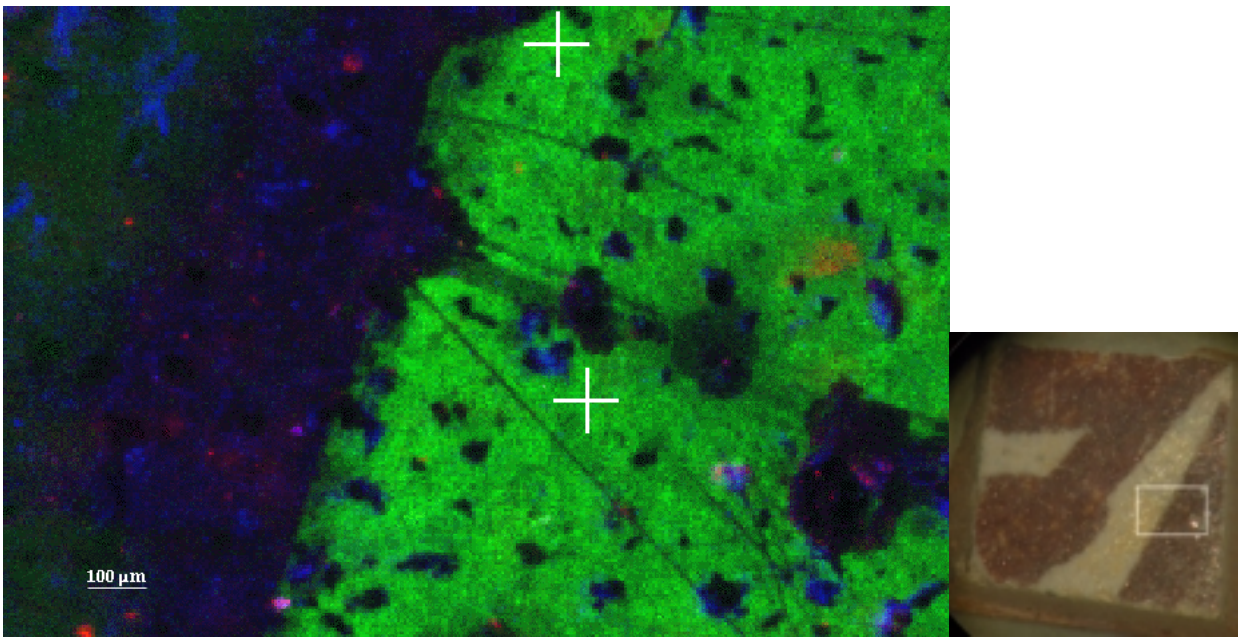

Figure 1. Tri-colour elemental map of a metal glazed strip of sample obtained from beamline 10.3.2, with (right) a larger scale visible light picture of the potsherd used. In the tri-colour map, copper is green, iron – red, calcium – blue. Shown are two locations from within the copper glaze from which copper K-edge EXAFS was recorded.

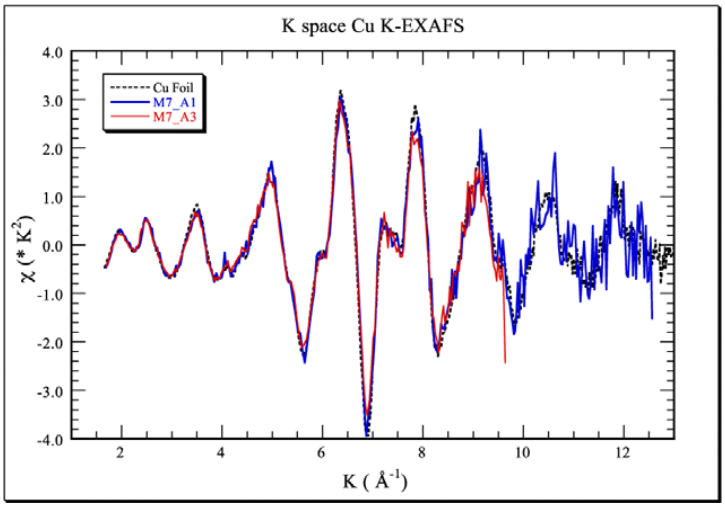

Figure 2. Cu K-edge EXAFS at two locations as shown in Figure 1 within the copper coloured part of a 'good' 14th century specimen with that obtained for a copper foil using the same instrument.

RESULTS

Examination of a number of specimens of both historical and recent providence has taken place and detailed analysis and interpretation of the results is still ongoing. Initial findings show that for good quality historical artifacts exhibiting distinct metallic glaze effects reduction to pure metal form has occurred. We present here Cu K-edge EXAFS from a 'good' Hispano Moresque 14th century specimen from Paterna (Valencia, Spain), illustrated in Figure 1. The Cu K EXAFS obtained from two sample areas within the copper glaze are shown in Figure 2, along with that for pure copper foil. Data acquisition times were of the order of 1 hour.

The fit of the experimental data to that of the pure foil is very good, demonstrating that not only was good reduction obtained in the firing process by the original potter, but also that the glaze itself has contained the copper effectively and prevented any subsequent oxidation through the centuries. Experimentally we also demonstrate the ability to collect good quality EXAFS data out to a K of 13 from small (20x20 microns) areas of these specimens, non-destructively and in reasonable time. EXAFS from "non-metallic" areas on other samples is more complex and requires further, more detailed analysis to fully interpret correctly. We hope to publish our findings shortly.

REFERENCES

[1] C.C.Tang, E.J.MacLean, M.A.Roberts, D.T.Clarke, A.J.N.W.Prag & E.Pantos. *J.Arch.Sci.* **28(10)**, 2001 pp1015-1024.

[2] R.B.Mason, & M.S.Tite. *Museum International* **46** 1994 pp33–37.

[3] J.Molera, T.Pradell, N.Salvadó & M.Vendrell-Saz. .*J A.n Ceram Soc.* **82 (10)**, 1999 pp2871–75.

[4] M.S.Tite, I.Freestone, R.Mason, J.Molera, M.Vendrell-Saz & N.Wood. REVIEW ARTICLE **"**Lead glazes in antiquity. Methods of production and reasons for use" *Archaeometry* **40(2)** 1998 pp241-2608.

[5] J.Pérez-Arantegui, J.Molera, A.Larrea, T.Pradell, M.Vendrell-Saz, I.Borgia, B.G.Brunetti., F.Cariati, P.Fermo, M.Mellini, A.Sgamellotti & C.Viti. "Luster pottery from the 13th to the 16th century: a nanostructured thin metallic film". *J. Am. Ceram. Soc.* **84(2)**, 2001 pp442-446.

[6] J.Molera, T.Pradell, N.Salvadó, & M.Vendrell-Saz, "Interaction between clay bodies and lead glazes" *J. Am. Ceram. Soc.* **84(5)**, 2001 pp1120-1128.

[7] J. Molera, M. Mesquida, J. Pérez-Arantegui, T. Pradell and M. Vendrell. "Lustre recipes from a medieval workshop in Paterna" *Archaeometry* **43(4)**, 2001 pp455-460.

This work is supported through proposal ALS00547. The Advanced Light Source is supported by the Director, Office of Science, Office of Basic Energy Sciences, Materials Sciences Division, of the U.S.Department of Energy under Contract No. DE-AC03-76SF00098 at Lawrence Berkeley National Laboratory. We also acknowledge CLRC-Daresbury Laboratory for supplying travel and subsistence funds.

Principal investigator: A.D.Smith, CLRC-Daresbury Laboratory, Warrington Cheshire WA4 4AD United Kingdom. Email: a.d.smith@dl.ac.uk. Telephone : +44-1925-603314

Monitoring anthropogenic metal released in the environment via X-ray fluorescence, absorption and diffraction at micrometer scales of resolution

A. Manceau[1,2], M.A. Marcus[1], N. Tamura[1], R.S. Celestre[1], A.A. MacDowell[1], R.E. Sublett[1], H.A. Padmore[1], M. Kersten[3]
[1]Advanced Light Source, Lawrence Berkeley National Laboratory, Berkeley, CA 94720
[2]Environmental Geochemistry Group, Hilgard Hall, University of California, Berkeley, CA 94720
[3]Geoscience Institute, Gutenberg University, 55099 Mainz, Germany

INTRODUCTION

Ferromanganese nodules are common in aquatic systems, including lacustrine and shallow marine environments, and also on the oceanic seafloor. They generally have a banded structure consisting of practically pure and alternating Fe- and Mn-rich layers separated by mixed Fe-Mn zones. This concretic onion-like growth pattern is attributed to intermittent oxidizing and reducing conditions. Accretion of ferromanganese nodules may cover time scales up to millions of years. The implication that they provide a continuously growing substrate with constant sorption efficiency for trace elements is the basis of a resuming interest for Fe-Mn nodules focusing on their possible use as a paleoproxy record for long-term environmental changes. Therefore, an idea was born to try and assess the metal fluxes into the ferromanganese nodules by dating individual nodule growth layers, and to compare these fluxes with the temporal variability in anthropogenic emissions. The prerequisite for such an approach is high-resolution profiling due to the slow accretion of the nodule material. Synchrotron-based micro-X-ray fluorescence (μSXRF) was applied to obtain in-situ trace element profiles of the necessary spatial resolution, as a basis for the evaluation of nodule accretion rates and for an assessment of their use for retrospective monitoring of excess metal input in the western Baltic Sea. Then, in-situ X-ray diffraction (XRD) and extended X-ray absorption fine structure (EXAFS) spectroscopy at the Mn and Zn K-edge were performed at the micrometer resolution to determine how anthropogenic Zn is taken up.

EXPERIMENTS

The examined nodule was collected in shallow water of the SW Baltic Sea where nodules are relatively fast-growing and enriched in metal contaminants, thus making them highly suitable to record the anthropogenic pollution in the last century. The sample was prepared as a micropolished 30 μm-thick thin section. The μXRD patterns of Fe- and Mn-pure layers were recorded on Beamline 7.3.3., and μEXAFS spectra were collected on Beamline 10.3.2. In both experiments, μSXRF maps were first recorded to image the Fe and Mn layers. All experiments were conducted with a beamsize of 15 (H) x 5 to 10 (V) μm.

RESULTS AND INTERPRETATION

The μSXRF element map of Fe and Mn (Fig. 1) shows the typically cuspate zebra-type band structure of the Fe-Mn concretions. The thickness of Mn-rich layers varies typically from 200 to 500 μm and that of the Fe-rich layers from about 100 to 200 μm. Of the trace elements investigated (Co, Ni, Cu, and Zn), Zn showed the most significant enrichment, with values in the outermost surface Mn layers of up to six-fold higher than those found in older core parts. Thus, the high-resolution Zn profiles provide the necessary temporal resolution for a dating method

analogous to dendrochronology. Assuming a continuous accretion of these relatively fast growing nodules (on average 20 µm yr^{-1}) over the last century, the Zn enrichment was assessed to have commenced in 1880/90, reflecting the enhanced heavy metal emissions with rising industrialization in Europe. µXRD patterns collected in Fe-rich regions (Fig. 2) contain only a broad and faint double hump with maxima at about 2.85 Å and 2.25 Å. The centroid of this hump is at about 2.5 Å as in poorly-crystallized two-line ferrihydrite (hydrous ferric oxide). Minor amounts of detrital quartz grains and silica particles (opal-A) were also detected by µXRD. The µXRD patterns taken in the Mn-rich layers look completely different consisting of a series of basal reflection peaks at 7.07 Å (001), 3.51 Å (002) and *hk*0 peaks at 2.46 Å (200) and 1.43 Å (110). These peak positions, together with the noteworthy asymmetrical shape of the (200) reflection, are characteristic of turbostratic hexagonal birnessite (δ-MnO_2).

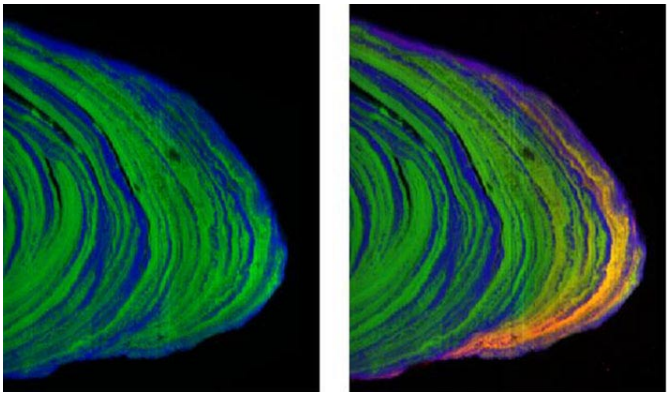

Figure 1. Synchrotron-based micro-X-ray radiation fluorescence (µSXRF) Fe and Mn maps of the outermost Fe and Mn layers of a ferromanganese nodule from the Baltic sea (6600 µm x 3780 µm, step size 15 µm, counting time 250 ms/pixel, red = Zn, green = Mn, blue = Fe, beamline: 10.3.2.). The onion-like structure of growth rims is clearly discernible as few hundreds µm thick Fe/Mn-rich bandings. Zn is exclusively associated with Mn, as indicated by the orange color of the Zn-containing Mn layers, and its concentration increases towards the surface.

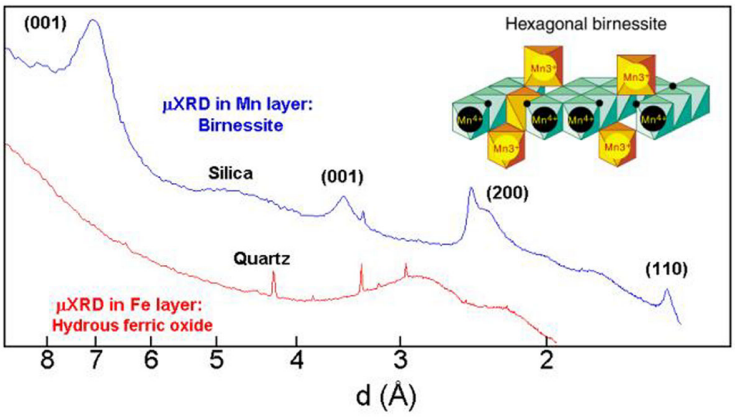

Figure 2. X-ray microdiffractograms collected in Mn (λ = 1.252 Å) and Fe (λ = 1.758 Å) layers. Mn is speciated as turbostratic hexagonal birnessite (δ-MnO_2), and Fe as hydrous ferric oxide. Quartz grains (sharp peaks) and silica particles (d ≈ 4.6 Å) were detected throughout the sample.

To determine the Zn sorption mechanism at the molecular-level, Zn K-edge µEXAFS spectra were collected in a Zn 'hot spot'. Qualitative information about the local structure of Zn can be obtained by comparing the unknown µEXAFS spectrum to reference EXAFS spectra from relevant model

compounds. The best spectral match was obtained with the Zn-sorbed birnessite reference, in which Zn is predominantly tetrahedrally, and secondarily octahedrally, coordinated and complexed above vacant sites of the manganese layer (Fig. 3). Comparison of radial structure functions (Fig. 3b) indicates that the Zn-O and Zn-Mn distances are both slightly, but significantly, shortened in the nodule sample, which is indicative of the presence of only ^{IV}Zn. The preferred formation of the ^{IV}Zn over the ^{VI}Zn complex presumably arises from the presence of aliovalent Mn^{3+} ions within the MnO_2 layer, because 4-fold coordinated Zn provides more positive charges to undersaturated oxygens (2+/4 = 0.5 v.u.) than a 6-fold coordinated Zn (2+/6 = 0.33 v.u.).

CONCLUSION

This study demonstrates the merit of deploying in parallel fluorescence, diffraction, and absorption studies at micrometer scales of resolution. This unprecedented combination of techniques allows the determination of the structural form of trace elements in heterogeneous matrices with an unequaled precision. Since much of nature and synthetic materials are heterogeneous on micron and sub-micron length scales, we anticipate that the synergistic use of µSXRF, µSXRD, and µEXAFS will have broad applications and add to the arsenal of analytical methods available in environmental and materials science.

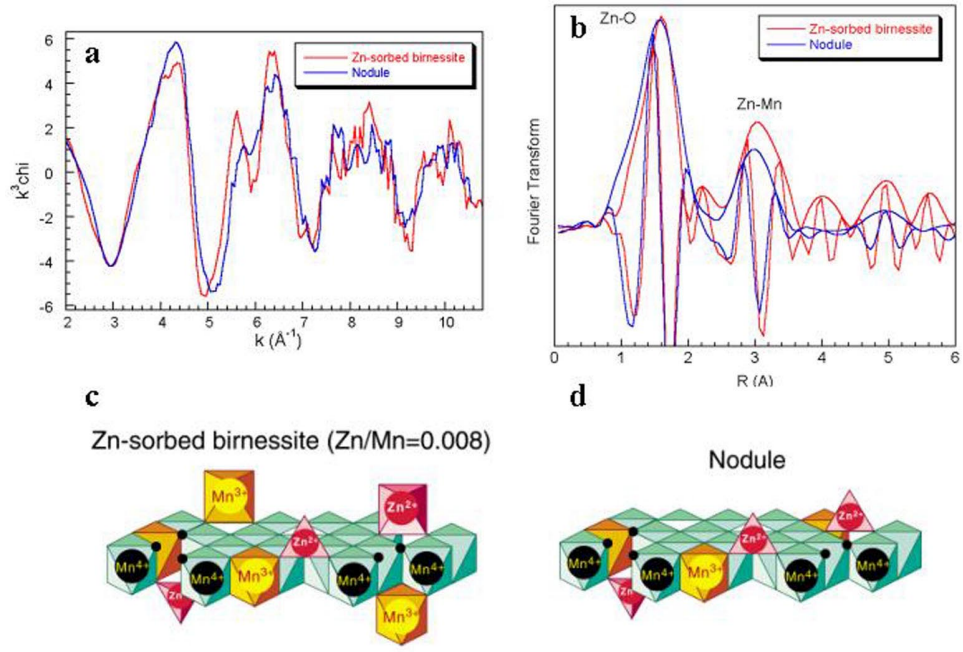

Figure 3. Zn K-dge µEXAFS spectrum and Fourier transform (modulus plus imaginary part) from a Zn 'hot spot' of the nodule rim presented in Fig. 1, compared to the Zn-edge data from a Zn-sorbed birnessite reference, in which Zn is sorbed as a mix of ^{IV}Zn and ^{VI}Zn complexes above vacant layer Mn sites. The unknown and reference data look similar, indicating that Zn are uptaken in a similar manner in the two compounds. However, Zn-O and Zn-Mn distances are clearly shorter in the natural sample because Zn is only four-fold coordinated.

This work was supported by the Director, Office of Energy Research, Office of Basic Energy Sciences, Materials Science Division, of the U.S. Department of Energy under Contract No. DE-AC03-76SF00098.

Principal investigator: Alain Manceau, Advanced Light Source, Ernest Orlando Lawrence Berkeley National Laboratory. Email: acmanceau@lbl.gov. Telephone: 510-643-2324.

Status report on Beamline 10.3.2

Matthew Marcus
Lawrence Berkeley National Laboratory, Berkeley, CA 94729

Beamline 10.3.2 has had a varied history, starting as an optics-development beamline on which new techniques could be explored, then evolving into an X-ray microprobe beamline. In its latest incarnation, it's a hard X-ray microprobe beamline optimized for environmental studies, with μEXAFS and μSXRF capabilities. Two years ago, the optics were changed to allow more flux at the cost of a bigger, but adjustable, spot size. The beamline came up to full user operation in November, 2001 and is now fully booked. While most of the users have been looking at speciation of metals in earth materials, there have also been projects in archeometry, osteology and microbiology.

The beamline can deliver white or monochromatic beam in a spot ranging from 16x6μm (full flux) down to 5x4μm FWHM. The energy range is 3-17keV. The optical layout consists of a horizontally deflecting 1:1 toroid, focusing to a slit, followed by optics inside the hutch, consisting of a vertically collimating parabolic mirror, 4 crystal monochromator, horizontally focusing ellipse and a vertically refocusing parabolic mirror. The optical layout is shown in Figure 1.

The sample is carried on a an XY stage with 10nm steps, and fluorescence radiation is detected by a 7-element Ge detector. Fluorescence mapping is done in a continuous-scan fashion in which the stage moves at a constant speed. The detector electronics allows one to define spectral regions of interest (ROIs) in which counts are accumulated. At fixed distance intervals, these counts are loaded into successive locations in the internal memory of the detector electronics. Thus, a line scan is built up without the need to step and repeat for each point. Successive line scans result in a two-dimensional fluorescence map.

These maps may be used to choose points at which to do EXAFS. This combination of fluorescence mapping and EXAFS is very useful in deciphering the structures of complex, inhomogeneous systems. Also, we have recently acquired a CCD for powder diffraction. Once that is integrated into the system, we will have the uniquely powerful combination of μSXRF, μEXAFS and μXRD, all available on the same sample in the same run.

An example of a fluorescence map from Alain Manceau's work is shown in Figure 2. This illustration shows gray-scale maps of the same ferromanganese soil nodule taken in the 'light' of several different elements. One can see, for instance, that areas high in Mn are low in Fe, that Ca exists mostly in the form of isolated mineral grains, and that As is found where Fe is. Such information, backed up with detailed analysis of EXAFS spectra, can shed light on how trace elements are sequestered in the environment, and hence add scientific rationale to the process of soil remediation.

For the April shutdown, we are planning to replace the 4-bounce monochromator with a 2-bounce, constant-height unit, which will yield a 3-10x flux improvement. Also, we plan to implement automatic mirror tuning, which will result in smaller spots and greater reliability. We now also have a Bruker SMART 6000 diffraction camera for the end station, and this will be fitted by summer '02. This will allow a range of diffraction experiments to be conducted, and will offer a similar capability to beamline 7.3.3, but with the addition of XAS. We are also examining the improvement in performance that would result from moving the system to a superbend. Improvements range from around 10 at 12 keV to nearly 100 at 20 keV, and would allow a much wider range of elements to be studied.

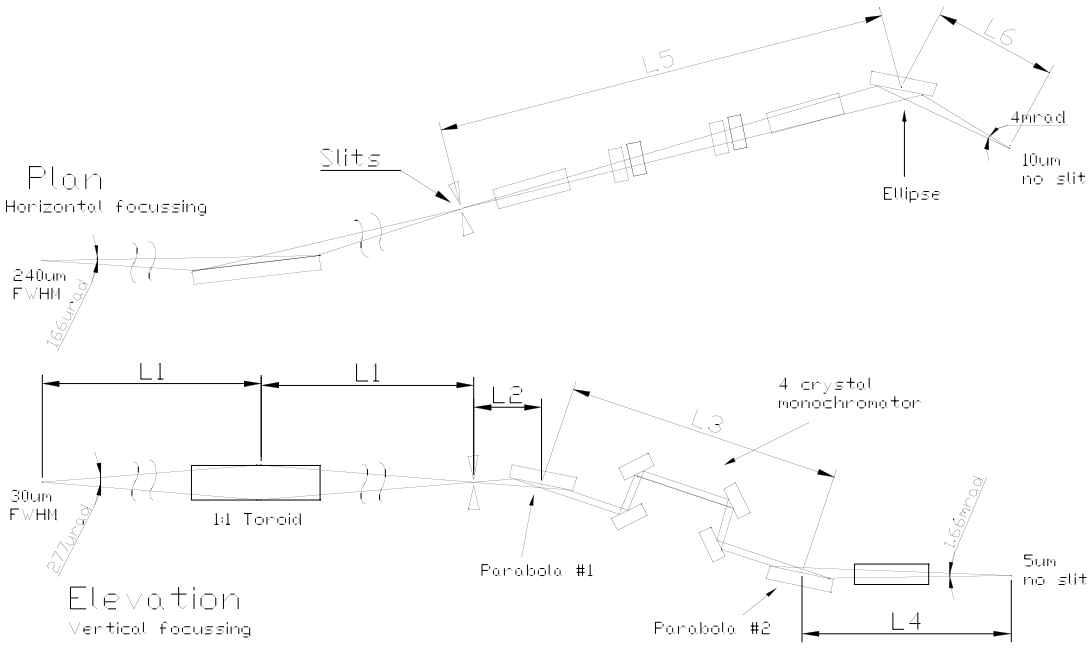

Figure 1. Optical layout. The dimensions L1..L6 and mirror types are as follows:

L1 = 14.75m	*Mirror*	*Type*	*Active area*
L2 = 1.44m	*M1*	*1:1 toroid*	*612 x 4.63mm*
L3 = 0.820m	*M2*	*V parabola*	*100 x 0.23mm*
L4 = 0.26m	*M3*	*V parabola*	*100 x 0.37mm*
L5 = 2.4m	*M4*	*H ellipse*	*100 x 0.66 mm*
L6 = 0.12m			

Mirror grazing angles = 4 mrads (coating = 8nm Rh on 20nm Pt on 5nm Cr)

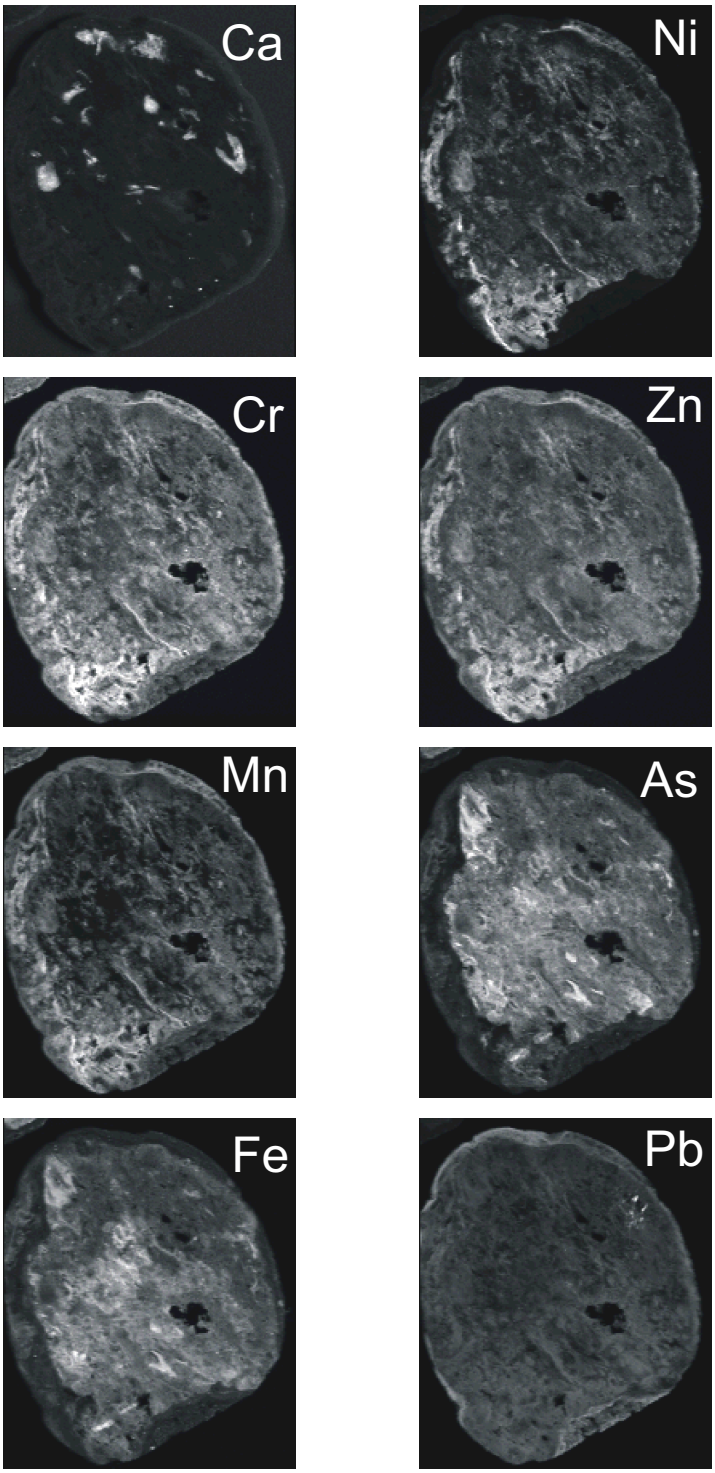

Figure 2. Elemental maps of a ferromanganese nodule. The As and Pb maps were taken below and above the Pb L_{III} edge, respectively, in order to separate the signals from these two elements.

This work was funded by the U.S. Department of Energy, Office of Science, Office of Basic Energy Sciences, Materials Sciences Division.

Contact person: Matthew A. Marcus, Advanced Light Source, Lawrence Berkeley National Laboratory.
Telephone: (510) 486-7604. Email: MAMarcus@lbl.gov.